P4A.5 **Three Hailstorms in the Kanto Plane, Japan**

Yoshimasa Takaya* and Masaru Ishibe

Meteorological Research Institute, Tsukuba, Japan

Mariko Mori

Aerological Observatory, Tsukuba, Japan

Takuya Tajiri and Tamotsu Misaki

New Tokyo Airport Service Center, Narita, Japan

1. Introduction

Located in central Japan, the Kanto Plain has a horizontal scale of 100 km. The Pacific Ocean borders the southern and eastern edges of the plain, while mountains up to two kilometers in altitude flank the northern and western perimeters. As summer sunlight warms the plain, cool, humid easterly sea breezes move in from the Kurile Current, and warm, humid southerly breezes arrive from the Kuroshio Current. The two fronts often converge near the center of the plain. In this paper, we show how the convergence line plays a major role in summer storm development in the Kanto Plain. Using C-band Doppler radar, aerological, and ground-based Automated Meteorological Data Acquisition System (AMeDAS) data, we analyze three hailstorms (15 July 1996, 24 May 2000, 11 May 2001) that developed as isolated supercells. Differences in character among the storms related to atmospheric environmental conditions and each storm's relative location to the convergence line. This paper also discusses precursor signals of downburst associated with midlevel convergence, and presents three-dimensional precipitation core figures using Vis5D visualization software.

2.Characteristics of the storms

2-1. Storm A (24 May 2000)

Scale marked this storm, which tracked 148 km, had an approximately 20-km overhang diameter seen at 45 dBZ.

Corresponding author address:
Dr. Yoshimasa Takaya,
Meteorological Research Institute
Tsukuba, 305-0052, JAPAN
E-mail: ytakaya@mri-jma.go.jp

2-2. Storm B (15 July 1996)

Intensity characterized Storm B. Hail diameters reached approximately 8 cm, winds gusted up to 46 m/s at the ground station, and the 15-km highest cloud top seen at 45 dBZ.

2-3. Storm C (11 May 2001)

Storm C featured the strongest sheer. The small supercell had 1-cm hail, and a cloud top of 7 km seen at 45 dBZ.

Table 1 summarizes the characteristics of each storm.

3. Estimated CAPE

In Japan, as the first aerological observation of stratification in a day is done in the morning (9 A.M. JST), it is difficult to predict afternoon storm outbreak. We replaced its surface data by using the ground station data located upstream side of and just before the outbreak of the storm and estimated CAPE. Then remarkable increase was obtained (see Table 1). Especially, storm B had the highest estimated value.

4. Propagation of the storms

In Fig. 1 the tracks of the storms are depicted on the map of Kanto-plane by six-minute intervals. Also environmental wind data are shown. The positions were determined as the center of mass of the storm area in which reflectivity is larger than 55dBZ in the lowest (0.7 degree elevation) PPI data. Storms were charted from the time mid-level mesocyclone appeared until a decay occurred and the 55dBZ reflectivity nearly disappeared.

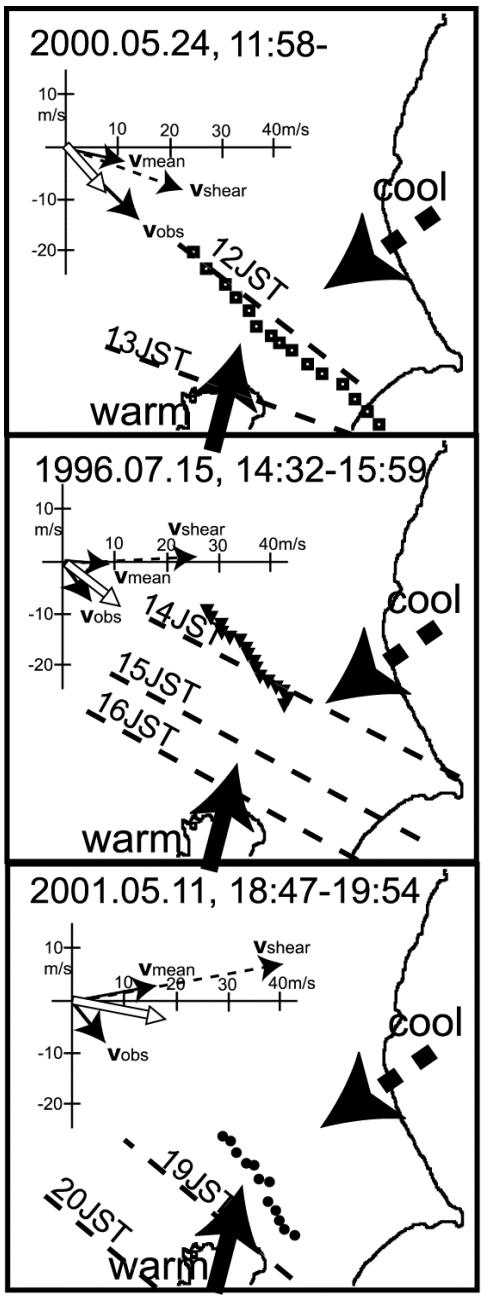

Figure 1: Storm paths over the Kanto Plain and environmental wind data. The dashed lines show the hourly convergence of cool easterly wind (thick broken arrow) and warm southerly wind (thick arrow). **V**mean represents non-pressure-weighted mean wind from the ground-6 km ASL. **V**shear is difference of winds between 5.5 km ASL and the ground level. Thick arrows represent propagation velocity (**V**obs), while white arrows indicate the predicted propagation velocity. Squares, triangles, and circles represent the propagation of storms A, B, and C, respectively. Scans were made approximately every six minutes.

Figure 1 does not show the end of Storm A, as the storm tracked beyond the radar's observation range. The broken lines represent the surface convergence line obtained by analyzing hourly AMeDAS data. The air masses had a 2 to 6° C temperature difference.

Bunkers *et.al* (2000) provided the following empirical equation for the propagation of a right-moving supercell:

$$\mathbf{V}_{\text{pred}} = \mathbf{V}_{\text{mean}} + D\frac{\mathbf{V}_{\text{shear}} \times \mathbf{k}}{|\mathbf{V}_{\text{shear}}|},$$

where $\mathbf{V}_{\text{mean}}$ and $\mathbf{V}_{\text{shear}}$ represent ground-6km non-pressure-weighted mean wind and wind difference between 5.5km and the ground, respectively. D is given as 7.5 m/s. $\mathbf{k}$ is a vertical-pointing unit vector. Although Bunkers *et.al*'s empirical equation predicted various propagation directions, all the study storms propagated approximately parallel to the convergence line. Only Storm A began and kept running just on the convergence line. The direction agreed with the direction predicted by the empirical formula. The other 2 storms remained in the cold air mass east of the convergence line. As shown in Figure 2, the configuration of the cool air mass to the east of the convergence line and the warm air mass to the west could produce a horizontal vortex tube.

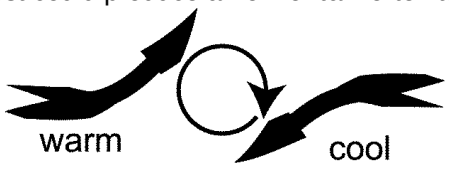

Figure 2: Horizontal vortex tube that may be produced by converging cool and warm air masses.

An updraft traveling along the convergence line, as in Storm A, might also experience strengthening of its existing cyclonic vortex.

5. Downbursts and their precursor signal

Three hours prior to the Storm A outbreak, aerological data from Tateno station, located several dozen kilometers from the outbreak point, showed two dry layers at about 4 and 7 km AGL.

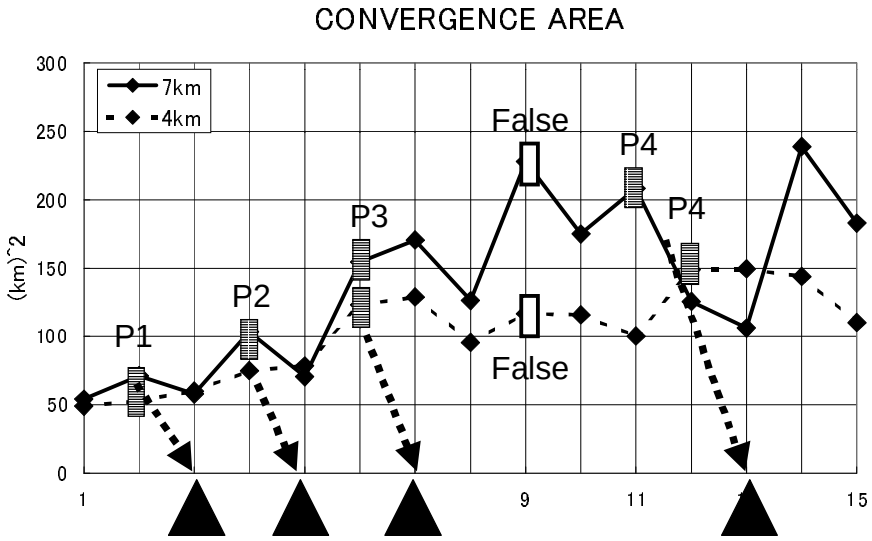

Figure 3: The changing strong (> 4 m/s/km) convergence area at 4 and 7 km AGL for Storm A. Four out of five precursor signals successfully predicted the outbreak of downbursts. The incorrect signal corresponded to a following mid-level updraft rather than a downdraft.

At these heights we analyzed the area of radial convergence stronger than 4 m/sec/km within a storm (Roberts and Wilson, 1989;Wolfson *et.al*, 1994) and Figure 3 plots the changing convergence area for Storm A. A 7-km curve shows 6 peaks. Downburst accompanied the first 3 peaks about six minutes after the recognition of the increase. No downburst followed the fourth peak. Reflectivity data show that the fourth peak related to mid-level updrafts (not shown here). Another downburst followed the fifth peak; a downburst may have also occurred after the sixth peak, but observations had ended.

6. Three dimensional storm shape

Vis5D software allows for three-dimensional storm diagrams. Figure 4 shows the developing precipitation core for Storm A at six-minute intervals. As the threshold is 55dBZ, this core could be composed of hail that seems to have 2 legs being quite similar to Fig. 5 in Knup (1996). At 12:05 JST the left leg (front-flank downdraft, Lemon *et.al*, 1979) had already touched down on the ground. At 12:11, a large hail stock, ready to fall, was observed in the upper core. At 12:17, the stocked hail fell, forming the right leg (rear-frank downdraft).

The following two figures show the storm ran with two legs. Real-time observations could have predicted the time and location of strong hail and downbursts.

7. Discussions and conclusions

The three hail storms ran along the direction of low level convergence line rather than in the direction predicted by Bunkers *et. al*. This indicates the importance of the convergence line in the Kanto Plane. Only Storm A obeyed the prediction and developed magnificently in scale, which indicates that if the directions predicted by Bunkers *et. al*. and of surface convergence line agree each other, the storm is expected to make strong development.

The estimated CAPE value related well to the storm intensity.

Strong convergence within the storm related to levels that aerological data indicated as dry layers, suggesting a possible downburst precursor signal.

New Vis5D visualization techniques also proved powerful in short-time hail and downburst forecasting.

This research found that combining aerological, surface observation network, and Doppler radar data provided good, very short-time forecasts.

	Item	unit	Storm A	Storm B	Storm B
			24 May 2000	15 July 1996	11 May 2001
Envionment	CAPE(00UCT)	J/kg	1000	2100	100
	CAPE(Estimated)	J/kg	2500	2900	500
	SREH	m^2/s^2	163	106	122
	Vshear	m/s	25	26	42
scale of storm	life time	min.	125	112	95
	length of track	km	148	60	83
	propagation speed	km/h	66	30	40
	diamter of midlevel mesocyclone	km	8.4	4.5	6
	cloudtop of 45dBZ	km	13	15	7
	diamete of overhang at 45 dBZ	km	20	5	5
intensity of storm	vorticity of midlevel mesocyclone	m/s/km	4.5	7.5	5.7
	velocity difference at midlevel mesocyclone	m/s	38	33	34
	speed of gust	m/s	31	46	13
	diamete of hail	cm	7	8	1

Table 1: Environmental conditions, scale, and intensity of the storms. Environmental conditions include observed (at 00 UTC) CAPE, estimated CAPE, system relative environmental helicity (SREH), and magnitude of the velocity difference between 5.5 km ASL and ground level. The following contributed to storm scale determinations: storm life (from mesocyclone appearance until precipitation at 2 km drops below 16 mm/h), propagation speed, mid-level mesocyclone diameter at the growth stage, cloud top height, and overhang diameter seen at 45 dBZ. Strength of vorticity, radial velocity difference in the mid-level mesocyclone, speed of ground station gusts, and hail diameter determined storm intensity.

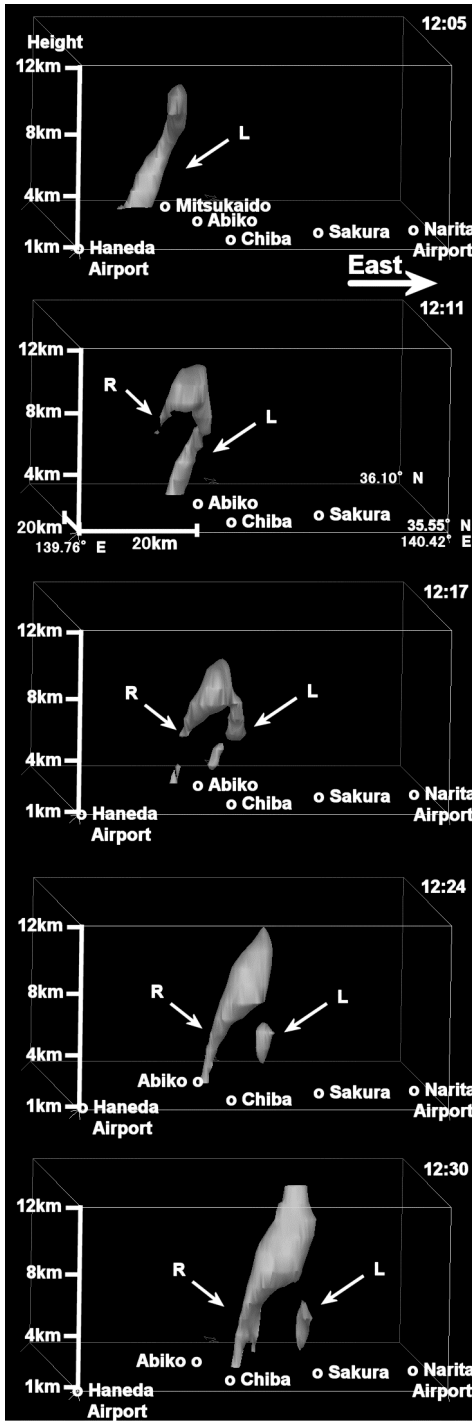

Figure 4: The development of Storm A represented by Vis5D based on five successive volume scans. The threshold of 55 dBZ indicates that the precipitation core may be composed of hail. The left leg touched down first. A huge hail stock formed in the upper air, and subsequently fell, forming the right leg.

References

Bunkers, M.J., B.A. Klimowski, J.W. Zeitler, R.L. Thompson, and M.L. Weisman, 2000: Predicting supercell motion using a new hodograph technique, Wea. Forecasting, **15**, 61-79.

Lemon, L.R., and C.A. Doswell III, 1979: Severe thunderstorm evolution and mesocyclone structure as related to tornadogenesis, *Mon. Wea. Rev.,* **107**, 1184-1197.

Knup, K.R. 1996: Structure and evolution of a long-lived, microburst-producing storm, *Mon. Wea. Rev.,* **124**, 2785-2806.

Roberts, R.D., and J.W. Wilson,1989: A proposed microburst nowcasting procedure using single-Doppler radar. *J.Appl.Meteor*., **28**, 285-303.

Wolfson, M.M., R.L. Delanoy, B.E. Forman, R.G. Hallowell, M.L. Pawlak, and P.D. Smith, 1994: Automated microburst wind-shear prediction, The Lincoln Laboratory Journal, **7**, 399-426.